AGU PUBLICATIONS

JGR

Journal of Geophysical Research: Space Physics

RESEARCH ARTICLE
10.1002/2014JA020658

Key Points:
- Optical emissions induced by *X*-mode HF pump wave
- Coexistence of optical emissions, ion and plasma lines, and irregularities
- Plasma turbulence induced by *X*-mode HF pump wave

Correspondence to:
N. F. Blagoveshchenskaya, nataly@aari.nw.ru

Citation:
Blagoveshchenskaya, N. F., T. D. Borisova, M. Kosch, T. Sergienko, U. Brändström, T. K. Yeoman, and I. Häggström (2014), Optical and ionospheric phenomena at EISCAT under continuous *X*-mode HF pumping, *J. Geophys. Res. Space Physics*, *119*, 10,483–10,498, doi:10.1002/2014JA020658.

Received 24 SEP 2014
Accepted 22 NOV 2014
Accepted article online 26 NOV 2014
Published online 18 DEC 2014

Optical and ionospheric phenomena at EISCAT under continuous *X*-mode HF pumping

N. F. Blagoveshchenskaya[1], T. D. Borisova[1], M. Kosch[2,3], T. Sergienko[4], U. Brändström[4], T. K. Yeoman[5], and I. Häggström[6]

[1]Department of Geophysics, Arctic and Antarctic Research Institute, St. Petersburg, Russia, [2]Physics Department, Lancaster University, Lancaster, UK, [3]South African National Space Agency, Hermanus, South Africa, [4]Swedish Institute of Space Physics, Kiruna, Sweden, [5]Department of Physics and Astronomy, University of Leicester, Leicester, UK, [6]EISCAT Scientific Association, Kiruna, Sweden

Abstract We present experimental results from multiinstrument observations in the high-latitude ionospheric F_2 layer at the EISCAT (European Incoherent Scatter Scientific Association) heating facility. The results come from a set of experiments, when an *X*-polarized HF pump wave at high heater frequencies ($f_H > 6.0$ MHz) was injected into the *F* region of the ionosphere toward the magnetic zenith. Experiments were carried out under quiet magnetic conditions with an effective radiated power of 458–548 MW. HF pumping was produced at different heater frequencies, away from electron gyroharmonic frequencies, and different durations of heater pulses. We show the first experimental evidence of the excitation of artificial optical emissions at red (630 nm) and green (557.7 nm) lines in the high-latitude ionospheric F_2 layer induced by an *X*-polarized HF pump wave. Intensities at red and green lines varied in the range 110–950 R and 50–350 R, respectively, with a ratio of green to red line of 0.35–0.5. The results of optical observations are compared with behaviors of the HF-enhanced ion and plasma lines from EISCAT UHF incoherent scatter radar data and small-scale field-aligned artificial irregularities from Cooperative UK Twin Located Auroral Sounding System observations. It was found that the *X*-mode radio-induced optical emissions coexisted with HF-enhanced ion and plasma lines and strong artificial field-aligned irregularities throughout the whole heater pulse. It is indicative that parametric decay or oscillating two-stream instabilities were not quenched by fully established small-scale field-aligned artificial irregularities excited by an *X*-mode HF pump wave.

1. Introduction

As a general rule, powerful HF radio waves with the ordinary polarization (*O* mode) are used for the modification of the *F* region of the ionosphere. Nonlinear interaction between powerful HF radio waves with the ordinary polarization (*O* mode) and the F_2 layer ionosphere plasma produces a large number of phenomena which are well documented [*Robinson*, 1989; *Gurevich*, 2007, and references therein]. The excitation of radio-induced optical emissions (RIOEs) is one of the impressive phenomena observed from HF modification experiments. The most common RIOEs, such as the red (630 nm) and green (557.7 nm) lines, were observed at different HF heating facilities at middle and high latitudes [see, for example, *Bernhardt et al*., 1989; *Brändström et al*., 1999; *Gustavsson et al*., 2001, 2002; *Pedersen and Carlson*, 2001; *Pedersen et al*., 2003, 2009; *Kosch et al*., 2007a; *Gustavsson and Eliasson*, 2008]. The threshold energies for the excitation of the O(^{1}D) and O(^{1}S) states of the atomic oxygen, responsible for the red and green lines, are 1.96 eV and 4.17 eV, respectively. The strongest artificial emissions are excited during HF pumping in the magnetic field-aligned direction [*Gurevich et al*., 2002; *Pedersen et al*., 2003; *Rietveld et al*., 2003; *Mishin et al*., 2005a].

It is believed that the main processes, responsible for the RIOE excitation at 630 nm and 557.7 nm under *O*-mode heating, are thermal electron heating and accelerated electrons. The former is produced mainly at the upper hybrid (UH) resonance altitude by the thermal parametric (resonance) instability, TPI [*Grach and Trakhtengerts*, 1975; *Vas'kov and Gurevich*, 1976], partly responsible for the excitation of red line emissions mainly for low heater frequencies below $f_H < 5$ MHz [*Gurevich et al*., 2004]. The latter is produced by the parametric decay instability, PDI [e.g., *Perkins et al*., 1974; *Fejer*, 1979; *DuBois et al*., 1990; *Stubbe et al*., 1992], at the reflection altitude of an ordinary polarized powerful HF radio wave when it decays into the electrostatic plasma waves such as a Langmuir wave (LW) and ion acoustic wave (IAW). The PDI acts over timescales of only a few milliseconds and typically affects the EISCAT (European Incoherent Scatter Scientific Association)

incoherent scatter spectrum at 930 MHz in the first few data dumps (each data dump is 6.4 s) [*Robinson*, 1989]. Furthermore, the IAW and LW are normally quenched within seconds when not pumping on an electron gyroharmonic frequency due to the fully established artificial field-aligned irregularities (FAIs) excited by the TPI, which scatter the pump wave thereby preventing further excitation of the PDI [e.g., *Stubbe*, 1996]. Langmuir waves may efficiently accelerate the electrons that, in turn, lead to the excitation of optical emissions at green line and at red line under heater frequencies above $f_H > 5$ MHz [*Gurevich et al*., 2004].

The behavior of HF-induced optical emissions is sensitive to the heater frequency relative to the electron gyroharmonic frequency, namely, when the heater frequency f_H equals to the upper hybrid frequency f_{UH} and multiple gyroharmonic frequency ($f_H = f_{UH} = nf_{ce}$, where f_{ce} is an electron gyrofrequency, and n is a multiple of the gyroharmonic). It was found that RIOEs are normally suppressed [*Leyser et al*., 2000; *Kosch et al*., 2002]. However, experiments at EISCAT/heating near the forth electron gyroharmonic [*Ashrafi et al*., 2007] and HAARP (High-frequency Active Auroral Research Program) in Gakona, Alaska, in the vicinity of the second gyroharmonic [*Mishin et al*., 2005b; *Gustavsson et al*., 2006; *Kosch et al*., 2007b] demonstrate that radio-induced optical emissions maximized at frequencies close to and just above the electron gyroharmonics.

An extraordinary (*X*-mode) powerful HF radio wave should not excite the upper hybrid resonance and Langmuir turbulence because its reflection height is below the UH resonance altitude and the reflection altitude of the *O*-polarized pump wave. Indeed, a comparison between *O*- and *X*-mode effects at the EISCAT HF heating facility clearly showed that the excitation of artificial field-aligned irregularities in the *F* region ionosphere occurs only during *O*-mode heating [*Robinson et al*., 1997]. The experiment reported by *Robinson et al*. [1997] was carried out at a heater frequency of f_H = 4.544 MHz which was below the critical frequency f_oF_2 ($f_H < f_oF_2$). Interesting observations of radio-induced optical emissions at red (630 nm) line from a HAARP experiment with simultaneous radiation of HF pump wave in *X* mode (f_H = 3.4 MHz) and *O* mode (f_H = 2.7 MHz) were reported by *Gustavsson et al*. [2009]. They demonstrated that the additional radiation of an *X*-polarized HF pump wave reduces the enhancement of the 630 nm emission, showing that an *X*-mode pump wave suppressed the nonlinear processes related to the TPI and driven by the *O*-mode HF pumping by raising the background plasma temperature by ohmic heating. Experiments carried out at the Sura heating facility (Nizhny Novgorod, Russia) also give evidence in favor of suppression the artificial plasma turbulences, both the parametric decay and thermal parametric instabilities, induced by the *O*-polarized HF pump wave (f_H = 4.3 MHz) due to the additional transmission of an *X*-mode wave (f_H = 4.8 MHz) [*Frolov et al*., 1999]. They found that the additional injection of an *X*-polarized HF pump wave leads, as a general rule, to the suppression of the stimulated electromagnetic emission (SEE) generation for different spectral components, induced by an intensity decrease of the Langmuir turbulence and small-scale artificial field-aligned irregularities. All experiments mentioned above were conducted at low heater frequencies ($f_H < 5.0$ MHz) and below the critical frequency of the F_2 layer ($f_H < f_oF_2$).

However, recent experimental data, obtained at the EISCAT (European Incoherent Scatter Scientific Association) HF heating facility, demonstrate that an *X*-polarized HF pump wave can also produce the artificial field-aligned irregularities (FAI), HF-enhanced ion, and plasma lines (HFIL and HFPL) in the EISCAT UHF radar spectra. The phenomena mentioned above were generated in the underdense ionosphere in the frequency band $f_xF_2 \geq f_H > f_oF_2$ for any heater frequencies in the range f_H = 4–8 MHz, where *O*-mode effects cannot be excited at all [*Blagoveshchenskaya et al*., 2011, 2013]. In addition, only for the higher heater frequencies ($f_H > 6$ MHz) can the HFIL and HFPL also be excited even in the overdense ionosphere, $f_H < f_oF_2$ [*Senior et al*., 2013]. Here f_oF_2 and f_xF_2 are the ordinary- and extraordinary-mode maximum plasma frequencies of the F_2 layer.

In this paper we show the first evidence of the excitation of artificial optical emissions at red (630 nm) and green (557.7 nm) lines in the ionospheric F_2 layer at the EISCAT heating facility induced by an *X*-polarized HF pump wave at high heater frequencies ($f_H > 6.0$ MHz), radiated parallel to the magnetic field direction. The results come from a set of experiments carried out at different heater frequencies and durations of heater pulses under quiet magnetic conditions. The optical results obtained are compared with behaviors of HF-enhanced ion and plasma lines from EISCAT UHF incoherent scatter radar data and small-scale field-aligned artificial irregularities from CUTLASS (Cooperative UK Twin Located Auroral Sounding System) observations.

2. Results From Multiinstrument Observations

2.1. Experiments

Multiinstrument observations have been made during the EISCAT heating campaign from 18 October to 3 November 2013. A large body of different types of HF pumping experiments has been carried out at the EISCAT site near Tromsø, Norway (69.58°N, 19.21°E). The ionospheric *F* region was perturbed by powerful continuous waves (CW) with *O* or *X* polarization from the EISCAT HF heater. The description and operational features of the heating facility are given by *Rietveld et al*. [1993]. Phased array 1, covering the frequency range between 5.4 and 8 MHz, with the beam width of 5–6° was utilized. The effective radiated power was varied between 450 and 650 MW. HF pumping was mainly produced in the magnetic field-aligned direction (magnetic zenith, 12°S). Here we report the experimental results from EISCAT HF pumping experiments on 22 and 25 October 2013 when *X*-polarized powerful HF radio waves were injected toward the magnetic zenith. We also include results from a similar EISCAT experiment on 19 October 2012. Experiments on 19 October 2012, 22, and 25 October 2013 have been carried out between 16 and 18 UT in solar maximum under quiet magnetic conditions. The values of solar Wolf number (*W*) and 3 h planetary magnetic index *Kp* were $W = 112$, 178, and 148, and $Kp = 0$, $1-$, and $1-$ on 19 October 2012, 22, and 25 October 2013, respectively. The effective radiated power (ERP) of the *X*-mode wave in the magnetic zenith varied between 458 and 548 MW for different experiments. HF pump waves were at frequencies of 6.2 and 7.1 MHz, which are away from the electron gyroharmonic frequencies, with 10 min on, 5 min off and 5 min on, 2.5 min off cycles.

On 19 October 2012 the heater frequency of $f_H = 6.2$ MHz was near the critical frequency, $f_H \approx f_oF_2$. We consider the phenomena under contrasting *O*/*X*-mode HF pumping from 17 to 17:30 UT. The *O*-mode HF pump wave was radiated from 17:01 to 17:11 UT, and then the *X*-mode HF heater pulse took place from 17:16 to 17:26 UT. In the course of the experiment on 22 October 2013, the values of $f_H = 7.1$ MHz were below and then near f_oF_2 ($f_H \leq f_oF_2$, overdense ionosphere). In this experiment only an *X*-mode HF pump wave was radiated from 16 to 18 UT with 10 min on, 5 min off pulses. On 25 October 2013 all three heater pulses at $f_H = 7.1$ MHz were produced in the underdense ionosphere, whereas two heater pulses at $f_H = 6.2$ MHz were made in the overdense ionosphere ($f_H < f_oF_2$). The experiment was conducted under *X*-mode HF pumping from 16:15 to 17 UT with 5 min on, 2.5 min off cycles alternating the heater frequency between 7.1 and 6.2 MHz from one heater pulse to another.

For radio-induced optical emissions (RIOEs) excited in the overdense ionosphere, it is important to estimate the possible leakage of the *O*-mode wave under *X*-mode pumping. The estimations have shown that the leakage of the *O* wave in the same direction (magnetic zenith) was about of 2.3–5 MW (less than 1% of full ERP). *Stubbe et al*. [1992] found for the EISCAT HF heater and UHF radar, the threshold of ERP = 17–35 MW was required to produce the Langmuir turbulence by an *O*-mode HF pump wave for typical *D* region absorption losses. It was also shown by *Bryers et al*. [2013] that the threshold value of 26 MW was needed to excite the TPI and PDI by an *O*-mode HF pump wave. Despite the fact that leakage of the *O* mode was small (ERP = 2–5 MW), we cannot completely exclude that it could have an impact on effects during *X*-mode pumping, when the heater frequency was below the critical frequency, $f_H < f_oF_2$.

2.2. Radio-Induced Optical Emissions

Radio-induced optical emissions at red (630 nm) and green (557.7 nm) lines were observed at the Tromsø site by the Digital All-Sky Imager 2 (DASI-2) and from remote sites by the Auroral Large Imaging System (ALIS) [*Brändström*, 2003] in Sweden. Both ALIS and DASI-2 detectors are 1024×1024 pixel, back-illuminated, thinned, high quantum efficiency, cooled slow-scan charge-coupled devices (CCDs). They are equipped with telecentric optics and filter wheels with narrowband interference filters for all the major auroral emissions. The field of view, filter sequence, and integration time can be varied according to the observation needs. The filters have the bandwidths of about 2.5 nm. The ALIS imagers are mounted in a remote controlled positioning system.

The first experiment, where the artificial *X*-mode emissions were generated, has been carried out at a heater frequency of 6.2 MHz on 19 October 2012 from 17:16 to 17:26 UT. Before an *X*-mode pulse, an *O*-mode HF heating pulse was made from 17:01 to 17:11 UT. Thus, we had a chance to compare the behaviors of the *O*- and *X*-mode radio-induced optical emissions. Artificial emissions at the red (630 nm) and green (557.7 nm) lines were imaged simultaneously at four remote ALIS stations located at Abisko (68°21′N; 18°49′E), Silkkimuotka (68°01′N; 21°41′E), Kiruna (67°50′N; 20°24′E), and Tjautjas (67°19′N; 20°45′E). ALIS was looking at

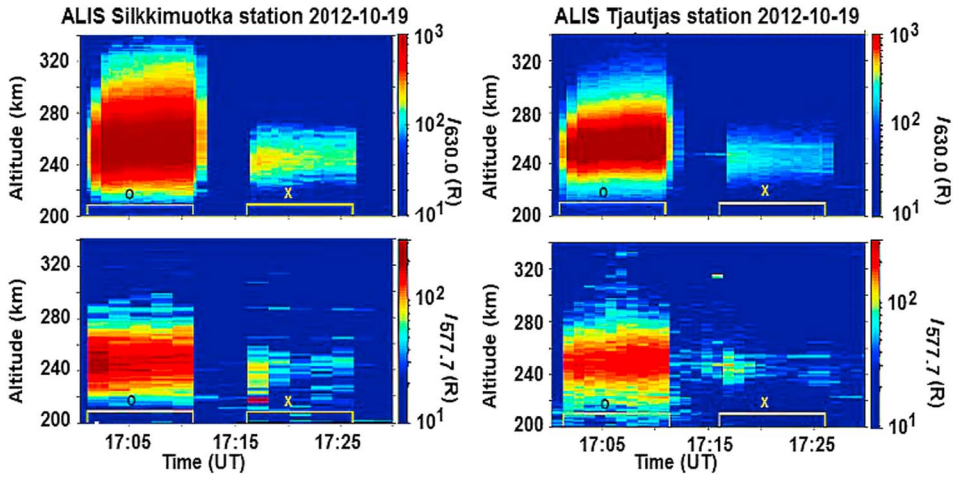

Figure 1. Contrasting *O*/*X*-mode radio-induced optical emissions imaged simultaneously at two remote ALIS stations located at Silkkimuotka (68°01′N; 21°41′E) and Tjautjas (67°19′N; 20°45′E) during the EISCAT heating experiment on 19 October 2012, showing the altitude distribution of intensities of red (630.0 nm) and green (557.7 nm) lines versus time (keograms). ALIS was looking at a volume above Tromsø and obtained one image every 10 s with an integration time of 6.5 s. The imager was running a filter sequence alternating between the emissions at 557.7, 630.0, and 844.6 nm. The HF pump wave was radiated at a heater frequency of 6.2 MHz toward the magnetic zenith (12°S) with *O*-mode (17:01–17:11 UT) and *X*-mode (17:16–17:26 UT) polarization. An *O*/*X*-mode HF pump wave with ERP ≈ 458 MW was radiated by 10 min on, 5 min off pulses beginning from 17:01 UT.

a volume above Tromsø and obtained one image every 10 s with an integration time of 6.5 s. The imager was running a filter sequence alternating between the emissions at 557.7, 630.0, and 844.6 nm. As an example, Figure 1 shows the ALIS optical observations at Silkkimuotka and Tjautjas stations for contrasting *O*/*X*-mode HF pumping on 19 October 2012. It is seen that HF-induced optical emissions at the red (630.0 nm) and green (557.7 nm) lines were generated through the whole 10 min continuous *X*-mode HF pump pulse, but they were not very strong. The intensity of emissions for the red and green lines was 110–150 and 50–75 R (Rayleighs) above the background, respectively. The intensity of *X*-mode RIOEs was less than the *O*-mode RIOEs, but there are differences between them. First, the emission peak altitude of red and green lines for *X*-mode RIOEs lies below the *O*-mode RIOEs by about 10 km. Second, the ratio of green line ($I_{577.7}$) to the red line ($I_{630.0}$) intensity is significantly higher for the *X*-mode RIOEs. The analysis of optical data exhibits the ratio values of about $I_{577.7}/I_{630.0} = 0.22–0.33$ for *O*-mode heater pulse, whereas for *X*-mode heating these values were of $I_{577.7}/I_{630.0} = 0.35–0.5$.

Unusually intense *X*-mode emissions were generated on 22 October 2013 from 16 to 18 UT when it was simultaneously observed at the Tromsø site by DASI-2 and at the remote ALIS Abisko station. Here the *X*-polarized continuous wave was radiated at 7.1 MHz using cycles of 10 min on, 5 min off. The optical observations are shown in Figure 2. Figure 2a shows the intensity of HF-induced optical emissions at red and green lines imaged by DASI-2 at the EISCAT site. Strong artificial red and green line emissions of 620–950 and 210–350 R above the background, respectively, and the ratio $I_{577.7}/I_{630.0} = 0.35–0.4$ were observed in every *X*-mode heater pulse between 16 and 18 UT. The altitude distribution of red and green line intensities versus time (keogram) obtained at ALIS Abisko station is depicted in Figure 2b. The maximum intensity of optical emissions at 630 and 557.7 nm was observed between 210 and 250 km altitude.

On 25 October 2013 radio-induced optical emissions at red and green lines were observed by DASI-2 from 16:15 to 17 UT at the Tromsø site. The *X*-polarized HF pump wave was radiated at frequencies of 7.1 or 6.2 MHz using 5 min continuous heater pulses and 2.5 min off. The critical frequency f_oF_2 gradually dropped from 6.9 MHz at 16.15 UT to 6.4 MHz at 17 UT. Thus, the heater pulses at 7.1 MHz occurred when the heater frequency f_H was above f_oF_2. In this case the intensity of 630 and 557.7 nm emissions was about 180–350 and 75–125 R above the background, respectively, and the ratio of $I_{577.7}/I_{630.0} = 0.35–0.4$. At $f_H = 6.2$ MHz the HF heating was produced when the heater frequency f_H was below f_oF_2. Here the intensities of red and green lines changed to $I_{630.0} = 120–150$ R and $I_{577.7} = 75–100$ R, respectively, with the ratio $I_{577.7}/I_{630.0} = 0.4–0.6$.

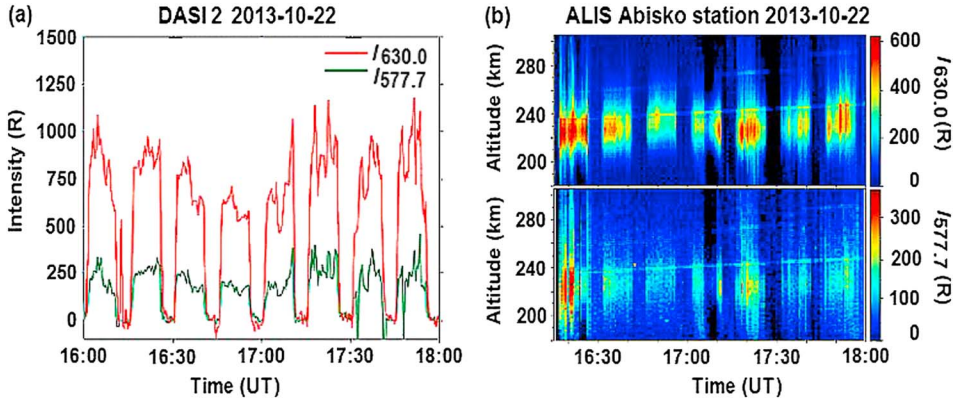

Figure 2. Radio-induced optical emissions during the EISCAT heating experiment on 22 October 2013. The *X*-mode pump wave was radiated at 7.1 MHz along the magnetic field from 16 to 18 UT by 10 min on, 5 min off pulses beginning from 16:01 UT. (a) The intensity of optical emissions at red (630.0 nm) and green (557.7 nm) lines imaged by the DASI-2 at the EISCAT site. (b) Altitude distribution of intensities of red (630.0 nm) and green (557.7 nm) lines versus time (keogram) obtained at the ALIS Abisko station. ALIS was looking at a volume above Tromsø and obtained one image every 10 s with an integration time of 6.5 s. The imager was running a filter sequence alternating between the emissions at 557.7, 630.0, and 844.6 nm.

2.3. HF-Induced Plasma Turbulence

Optical measurements were accompanied by observations from the EISCAT UHF incoherent scatter radar at 930 MHz, described by *Rishbeth and Van Eyken* [1993] located in the immediate vicinity of the HF heater. The radar data are processed by the Grand Unified Incoherent Scatter Design and Analysis Package [*Lehtinen and Huuskonen*, 1996]. The UHF radar allows the detailed study of longitudinal plasma oscillations such as Langmuir and ion acoustic waves. Strong ion acoustic and Langmuir waves (IAW and LW) are produced by the parametric decay instability (PDI) near the reflection level of the HF heater wave. Both IAW and LW are directly detected by incoherent scatter radar colocated with the HF heating facility as HF-enhanced ion and plasma lines (HFILs and HFPLs) in the radar spectra. We have calculated the power spectra of ion and plasma lines and determined the intensities of downshifted and upshifted HF-enhanced ion lines and the downshifted HF-induced plasma lines. We note that the UHF radar measured only the downshifted plasma line. The power spectra were calculated from the so-called "raw" data with altitude resolution of 3 km and 30 s integration time. Such spectra show the distribution of power of HF-induced ion (or plasma) lines in the frequency band corresponding to the ion acoustic (or Langmuir) waves.

On 19 October 2012 from 17:01 to 17:26 UT, the UHF radar was scanned in elevation angle in the sequence of 76-77-78-79-80° (2 min for every angle step). The magnetic field-aligned direction at Tromsø corresponds to 78°. In this period contrasting *O*/*X*-mode HF pumping was conducted, and the *O*/*X*-mode optical emissions at the red and green lines were excited. Figure 3 shows the temporal variations of the undecoded downshifted plasma line intensities and altitude-temporal behavior of the backscattered power (raw electron density), which is indicated by the appearance of ion lines in the radar spectra. As seen in Figure 3, intense HF-induced plasma lines throughout the whole CW heater on pulse were observed for *X*-mode injection (17:16–17:26 UT), whereas *O*-mode heating (17:01–17:11 UT) produced only a short weak HFPL in response to the turning on of the HF heater. The UHF radar data exhibit also the excitation of intense *X*-mode HF-enhanced ion lines (HFILs), which were much stronger than in the preceding *O*-mode heater pulse. Figure 4 illustrates in more detail ion line spectra for *O*- and *X*-mode heater pulses on 19 October 2012. By comparing cases for *O*- and *X*-mode heater pulses, it is evident that HFILs induced by an *X*-polarized pump wave are excited about 10 km below that of *O*-mode ion lines. This is in the agreement with the reflection heights for *X*- and *O*-polarized HF pump waves. An *O*-mode HF pump wave is reflected from the ionosphere where the heater frequency f_H becomes equal to the local plasma frequency f_0, ${f_H}^2 = {f_0}^2$. *X*-mode reflection occurs at the height where the local plasma frequency is determined as ${f_0}^2 = f_H\,(f_H - f_{ce})$, where f_{ce} is the electron gyrofrequency. *X*-mode reflection is below the *O*-mode reflection height. It is also seen in Figure 4 that the intensities of HF-induced ion lines in the *X*-mode heater pulse were higher by 3 orders of magnitude in comparison with the *O*-mode pulse. The other unusual feature is a peak at zero frequency (central peak) of

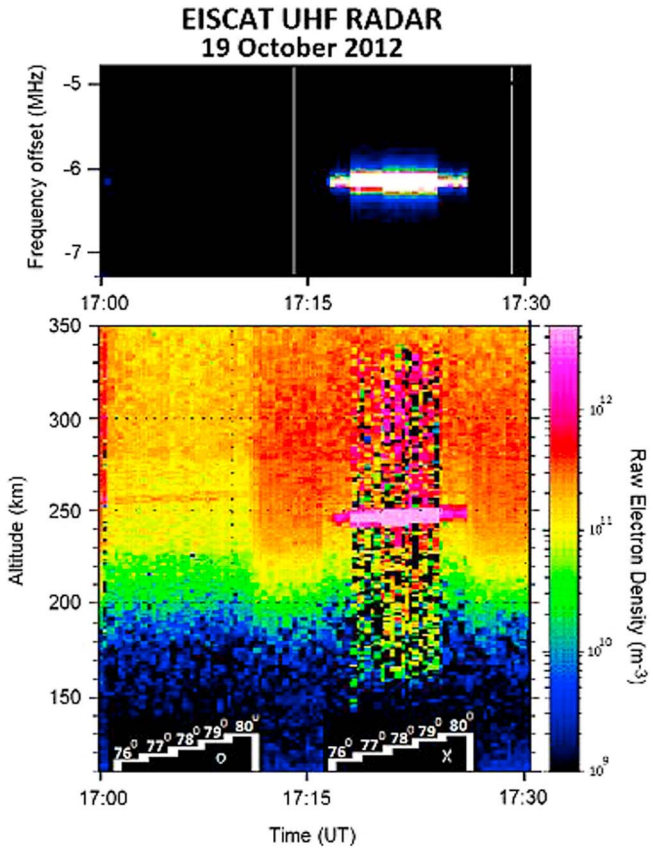

Figure 3. Temporal variations of the undecoded downshifted plasma line intensities, (top) range of altitudes of 209–383 km, and (bottom) altitude-temporal behavior of the backscattered power labeled as raw electron density obtained from the EISCAT UHF radar observations for contrasting *O*/*X*-mode heating on 19 October 2012 from 17 to 17:30 UT. HF heater details are the same as in Figure 1. The UHF radar was scanned in elevation angle in the sequence of 76-77-78-79-80° (2 min at every angle step). *O*/*X*-mode heater pulses and elevation angles of UHF radar are marked on the time axis.

the normally twin-peaked ion line spectra obtained by injection of an *X*-mode HF heater wave (see Figure 4b). The appearance of such a nonshifted spectral component is a signature of the oscillating two-stream instability (OTSI) in the incoherent radar spectra. HF-induced plasma and ion lines for *X*-mode pulses were excited over a wide range of altitudes with the maximum near the reflection height of the *X*-polarized HF pump wave. Moreover, they were the most intense in a narrow-angle beam between 77 and 79° (around the magnetic zenith).

Intense HF-induced plasma and ion lines were generated on 22 October 2013 in all 10 min CW heater pulses over 2 h between 16 and 18 UT. The UHF radar was pointing along the magnetic field-aligned direction. The HF-induced plasma and ion lines from the EISCAT UHF radar observations on 22 October 2013 are shown in Figures 5 and 6. Figure 5 illustrates the temporal variations of the undecoded downshifted plasma line intensity, the altitude-temporal behavior of the downshifted plasma line power, and the backscattered power (raw electron density). Figure 6 presents the maximum power of HF-enhanced ion lines (upshifted and downshifted) and the downshifted plasma lines at fixed altitudes. The power of the HFILs and HFPLs was 2–4 orders of magnitude above the background level over a wide height extent throughout the whole CW heater pulses. For comparison, we also show in Figure 5 the HF-induced ion line intensities at the altitude of 361 km, where only very weak enhancements were observed.

Intense HF-induced ion and plasma lines were also generated during *X*-mode heating at 6.2 and 7.1 MHz on 25 October 2013 from 16:15 to 17 UT. Similar to the 22 October 2013 event, the UHF radar was also operating in the magnetic field-aligned direction. The main difference between 22 and 25 October for the heater frequency f_H = 7.1 MHz was the relation between f_H and the critical frequency of the F_2 layer, f_oF_2.

It is interesting to compare the HF-induced plasma and ion lines at the same heater frequency (f_H = 7.1 MHz), when it is below and above the critical frequency f_oF_2 ($f_H < f_oF_2$ and $f_H > f_oF_2$). We have compared an *X*-mode heater pulse on 22 October 2013 from 16:16 to 16:26 UT (the heater frequency was below the critical frequency, $f_H < f_oF_2$) and on 25 October 2013 from 16:53:30 to 16:58:30 UT (the heater frequency was above the critical frequency, $f_H > f_oF_2$).

Figures 7 and 8 show the ion line spectra at fixed altitudes and in the altitude-frequency coordinates, respectively, for these two heater pulses obtained from UHF radar measurements. Altitude profiles of the downshifted and upshifted ion line intensities as well as the downshifted plasma line for the same heater pulses are depicted in Figure 9. As a whole, the behavior of HF-induced ion and plasma lines are very similar in both cases. However, the altitude range occupied by the HFILs (downshifted and upshifted) and HFPLs is

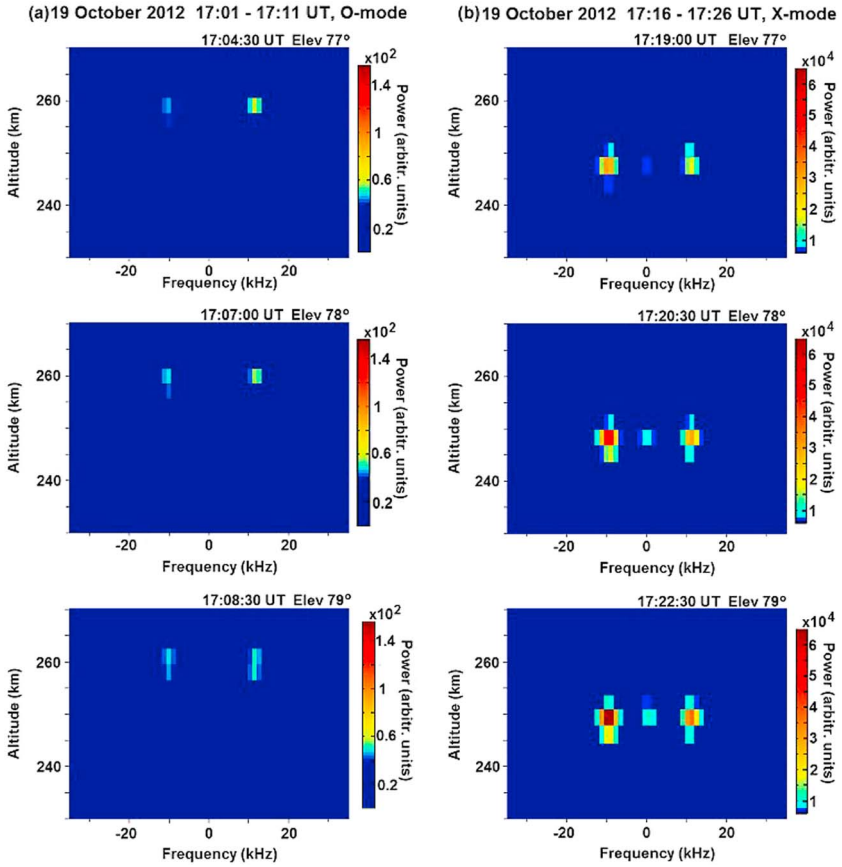

Figure 4. Ion line spectra in altitude-frequency coordinates obtained from the EISCAT UHF radar observations for elevation angles 77, 78, 79° with 3 km altitude resolution and 30 s integration time for contrasting *O*/*X*-mode heating at 6.2 MHz on 19 October 2012. (a) Ion line spectra for *O*-mode HF heater pulse from 17:01 to 17:11 UT at 17:04:30 UT (77°), 17:07:00 (78°), and 17:08:30 UT (79°). (b) Ion line spectra for *X*-mode HF heater pulse from 17:16 to 17:26 UT at 17:19:00 UT (77°), 17:20:30 (78°), and 17:22:30 UT (79°). HF heater details are the same as in Figure 1. The UHF radar in every HF heater pulse was scanned in elevation angle in the sequence of 76-77-78-79-80° (2 min at every angle step).

wider for the case when $f_H > f_oF_2$. An interesting feature was identified in the altitude distribution of the downshifted ion line intensities. Two power maxima at different altitudes (the bottomside echo and topside echo) can be recognized in both cases, when $f_H < f_oF_2$ and $f_H > f_oF_2$. The bottomside echo is seen near the reflection level of the *X*-mode HF pump wave (about 225 km), while the topside echoes were about 12 and 30 km higher for heater pulses under $f_H < f_oF_2$ and $f_H > f_oF_2$, respectively. Similar features were observed almost in all HF pump pulses at $f_H = 7.1$ MHz on 22 and 25 October 2013. The nonshifted spectral component at zero frequency in the ion line spectra, which can be clearly identified at $f_H = 6.2$ MHz on 19 October 2012, was not observed at $f_H = 7.1$ MHz on 22 and 25 October 2013.

2.4. Signals Backscattered From Artificial Field-Aligned Irregularities

The CUTLASS (Super Dual Auroral Radar Network (SuperDARN)) HF coherent radar [*Lester et al.*, 2004] at Hankasalmi, Finland (62.3°N; 26.6°E) was used for detecting the signals backscattered from artificial field-aligned irregularities (FAIs) excited by the *X*-mode wave. CUTLASS operated at three frequencies between 13 and 20 MHz with a range gate resolution of 15 km and integration time of 3 s. Beam 5 (3.3° width) oriented over the EISCAT HF heater was utilized in all experiments.

CUTLASS measurements on 19 October 2012, 22, and 25 October 2013 clearly demonstrate the generation of strong *X*-mode FAIs coexisting with the artificial optical emissions and HF-induced ion and plasma lines. CUTLASS radar backscatter at 13, 16, and 18 MHz, corresponding to FAI transverse (to the magnetic field) scales of $l_\perp \approx 11.5$, 9, and 8 m, on 22 October 2013 is depicted in Figure 10. We see that strong signals

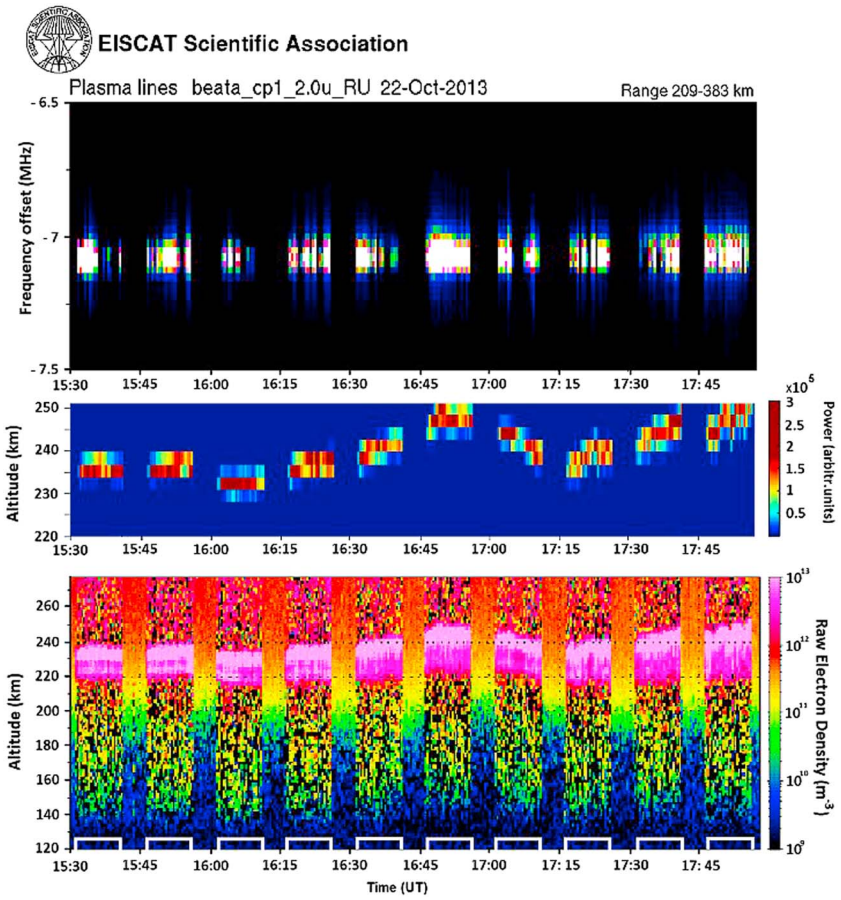

Figure 5. Temporal variations of the undecoded downshifted plasma line intensities, (top) range of altitudes of 209–383 km, (middle) the altitude-temporal behavior of the downshifted plasma line power, and (bottom) the backscattered power, labeled as raw electron density obtained from the EISCAT UHF radar observations for *X*-mode heating on 22 October 2013 from 15:30 to 18 UT. HF heater details are the same as in Figure 2. The UHF radar was pointing in the magnetic field-aligned direction (12°S). *X*-mode heater pulses are marked on the time axis.

backscattered from FAIs were observed at all frequencies in every heater pulse. The strongest artificial backscatter occurred at the highest operational frequency of 18 MHz. In addition, the size of the backscattered region increases with higher-radar frequency. The spatial size of region occupied by FAIs with the larger scale of $l_{\perp} \approx 11.5$ m took four range gates (60 km), while FAIs with $l_{\perp} \approx 8$ m were seen over seven range gates (105 km).

2.5. Other Phenomena

In the course of the experiments stimulated electromagnetic emission (SEE) measurements were conducted at Tromsø with a spectrum analyzer in a frequency band of 200 kHz with the resolution of 20 Hz. This allows for investigating the main SEE spectral features in the kilohertz frequency band. The common SEE spectral feature under *O*-mode HF pumping, for heater frequencies away from electron gyroharmonic frequencies, is the downshifted maximum (DM) spectral component. On 19 October 2012 during the *O*-mode heater pulse at 6.2 MHz an intense DM component was observed in the SEE spectra at a frequency downshifted from the pump frequency by $\Delta f_{DM} \approx 12$ kHz. The DM peak intensity typically occurs at $\Delta f_{DM} \approx 2 \times 10^{-3} f_H$, where f_H is a pump frequency [*Stubbe et al.*, 1984]. It has been proposed by *Leyser* [2001] that upper hybrid (UH) and low-hybrid (LH) oscillations are likely to be important in the DM generation. SEE measurements in the course of *X*-mode heater pulses clearly demonstrate the absence of the DM component in the SEE spectra.

We have also analyzed the altitude-temporal behavior of the plasma parameters from the EISCAT UHF incoherent scatter radar observations, such as the electron density, *Ne*, the electron and ion temperatures,

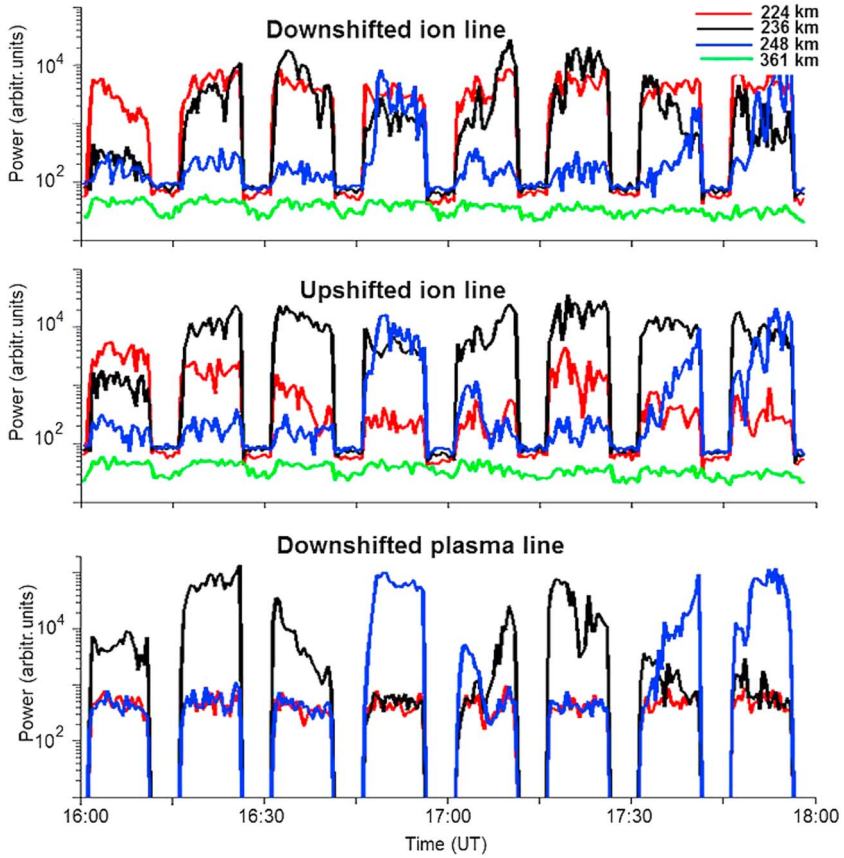

Figure 6. Time series of the maximum power of the HF-enhanced downshifted and upshifted ion lines and downshifted plasma lines at fixed altitudes of 224, 236, 248, and 361 km on 22 October 2013. Powers were determined as the maximum in the ion line and plasma line spectra obtained with 3 km altitude resolution and 30 s integration time. HF heater details are the same as in Figure 2.

Te and *Ti*, and the ion velocity, *Vi*. On 19 October 2012 in the course of the *O*-mode heater pulse from 17:01 to 17:11 UT strong thermal heating accompanied by the generation of the ion outflows occurred. The values of *Te* increased from about 1000 K just before the heater-on to 3000 K during the heater pulse at altitudes of about 350–400 km. The strongest *Te* enhancements were observed in the magnetic field-aligned direction (between 77 and 79° elevation angles of the UHF radar). Ion velocities *Vi* reached 230 ms^{-1} at the altitude of 523 km. The behaviors of plasma parameters under an *X*-mode heating are different from those observed under *O*-mode injection. The typical feature of *X*-mode heating was the strong apparent electron density enhancements in the magnetic field-aligned direction in a wide altitude range up to the upper limit of UHF radar measurements (600 km). Such strong *Ne* increases were accompanied by not too large electron temperatures enhancements as compared with *O*-mode effects. The ion outflows were not generated under *X*-mode heating. There were no significant changes in the ion temperatures for both *O*- and *X*-mode heating. It is important that intense ion acoustic waves were excited under *X*-mode HF pumping. It is not possible to perform proper estimations of the *Ne* and *Te* in the altitude range occupied by HF-enhanced ion acoustic waves due to a high residual to the fitting. On 22 October 2013 intense ion acoustic waves were excited at altitudes from 220 to 250 km (see Figures 6 and 9a). On 25 October 2013 the HF-enhanced ion lines occurred from 220 to 280 km (see Figure 9b). However, the UHF radar observations exhibit very large apparent *Ne* increases by 50–70% above the background *Ne* level in the altitude range above the region occupied by HF-enhanced ion lines. Electron temperature increased from about 1000 K just before the *X*-mode heater pulse to only 1300 K at the altitude of 350 km during the heater pulse. A similar behavior of the *Ne* and *Te* was also observed on 19 October 2012 from 17.16 to 17.26 UT during an *X*-mode heater pulse.

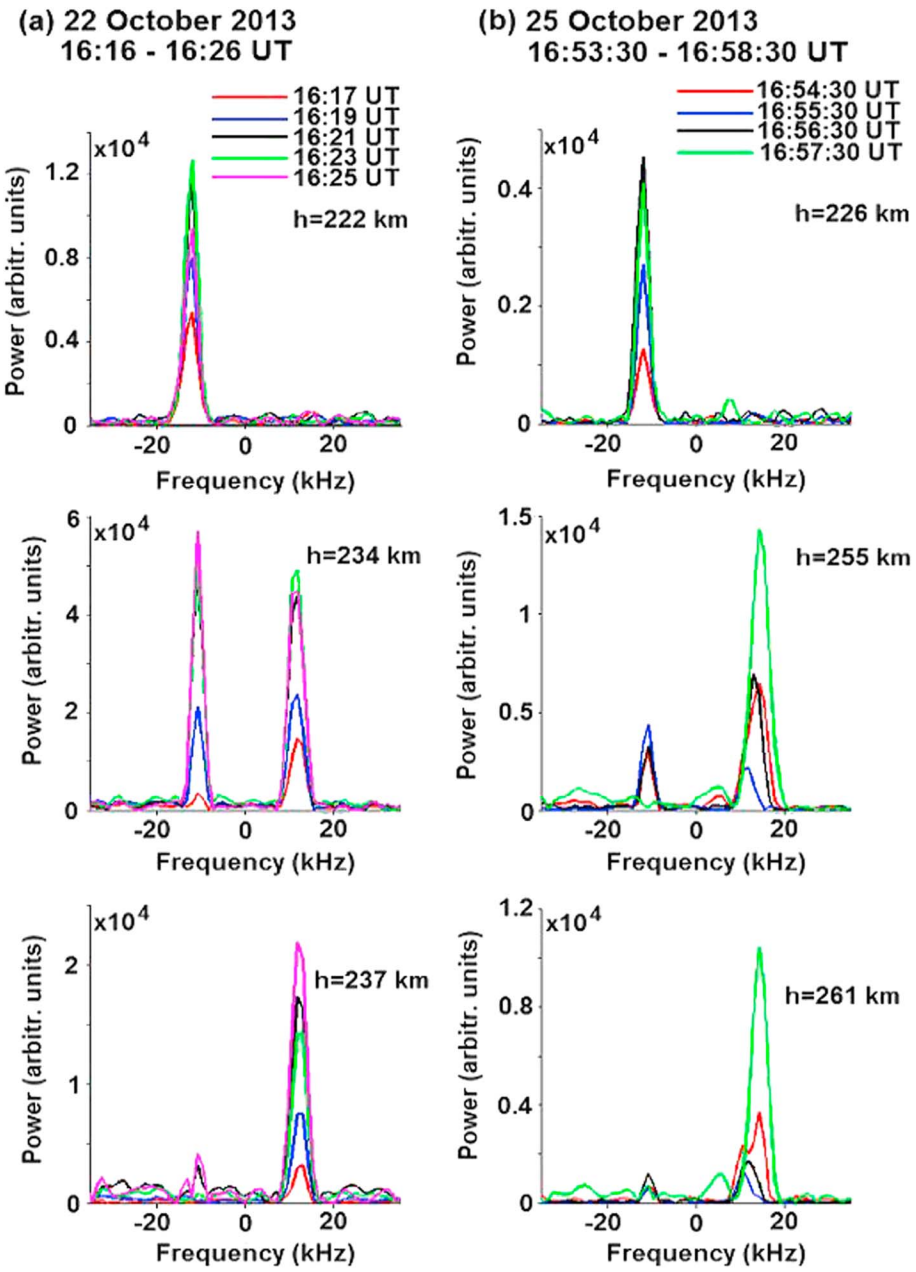

Figure 7. Ion line spectra at fixed altitudes for two HF heater pulses when the heater frequency was below and above the critical frequency ($f_H < f_oF_2$ and $f_H > f_oF_2$, respectively) obtained from UHF radar measurements in the magnetic field-aligned direction with 3 km altitude resolution and 30 s integration time. In both cases an *X*-mode pump wave was radiated at 7.1 MHz toward the magnetic zenith. (a) Ion line spectra on 22 October 2013, for the heater pulse from 16:16 to 16:26 UT ($f_H < f_oF_2$) at altitudes of 222, 234, and 237 km for times 16:17, 16:19, 16:21, 16:23, and 16:25 UT. (b) Ion line spectra on 25 October 2013, for heater pulse from 16:53:30 to 16:58:30 UT ($f_H > f_oF_2$) at altitudes of 226, 255, and 261 km for 16:54:30, 16:55:30, 16:56:30, and 16:57:30 UT.

3. Discussion

We have demonstrated for the first time, from a set of repetitive experiments under very quiet magnetic conditions, that an *X*-polarized HF pump wave, injected into the F_2 layer toward the magnetic zenith, can generate the radio-induced optical emissions (RIOEs) at the red (630 nm) and green (557.7 nm) lines. It was shown that RIOEs were generated at high heater frequencies of 6.2 and 7.1 MHz, lying away from electron gyroharmonic frequencies, under different relations of heater frequency f_H to the critical frequency f_oF_2

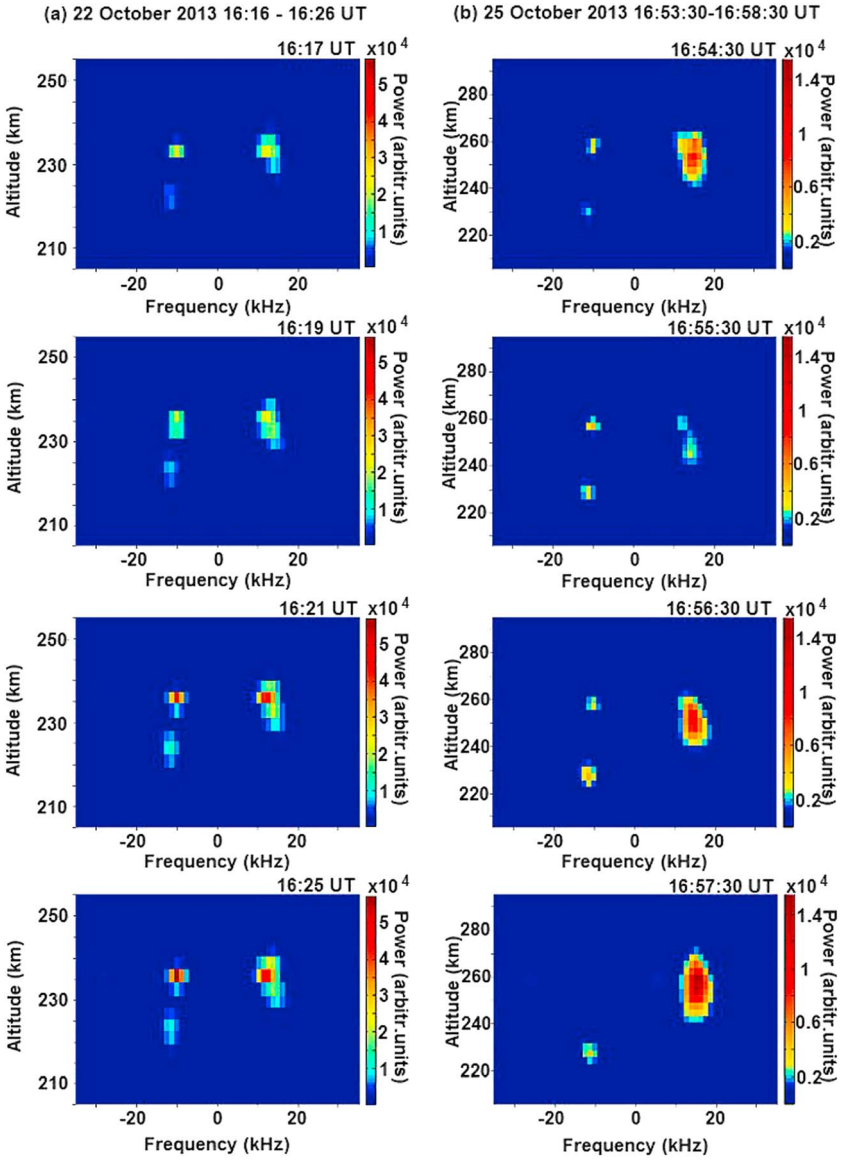

Figure 8. Ion line spectra in altitude-frequency coordinates obtained from EISCAT UHF radar observations for the same HF heater pulses as in Figure 7. (a) Ion line spectra on 22 October 2013, for HF heater pulse from 16:16 to 16:26 UT ($f_H < f_oF_2$) at 16:17, 16:19, 16:21, and 16:25 UT. (b) Ion line spectra on 25 October 2013, for HF heater pulse 16:53:30–16:58:30 UT ($f_H > f_oF_2$) at 16:54:30, 16:55:30, 16:56:30, and 16:57:30 UT.

($f_H > f_oF_2$, $f_H \approx f_oF_2$, $f_H < f_oF_2$). The intensities at red and green lines in different experiments varied through a range of 110–950 R and 50–350 R, respectively. The ratio of green ($I_{577.7}$) to red ($I_{630.0}$) line was $I_{577.7}/I_{630.0} = 0.35–0.5$. The distinctive feature of *X*-mode artificial optical emissions is their coexistence with the intense HF-enhanced ion and plasma lines, the strong small-scale artificial field-aligned irregularities, and apparently enhanced electron density in the magnetic field-aligned direction through the whole heater pulse. Such strong and repeatable phenomena induced by an *X*-mode HF pumping are very unusual.

On 19 October 2012, when the heater frequency f_H was near the critical frequency f_oF_2 ($f_H \approx f_oF_2$), alternating *O*/*X*-mode heating was produced during 17–17:30 UT. We have to keep in mind that the *O*-mode HF pump wave is actually reflected slightly below the critical frequency when it is radiated toward the magnetic zenith. Hence, the *O* wave could be injected at a frequency slightly above the f_oF_2 and still be reflected. The comparison between the *O*- and *X*-mode radio-induced optical emissions clearly showed the differences between them. As it was shown in section 2.2, the ratio of green to red lines for *O*-mode heating was

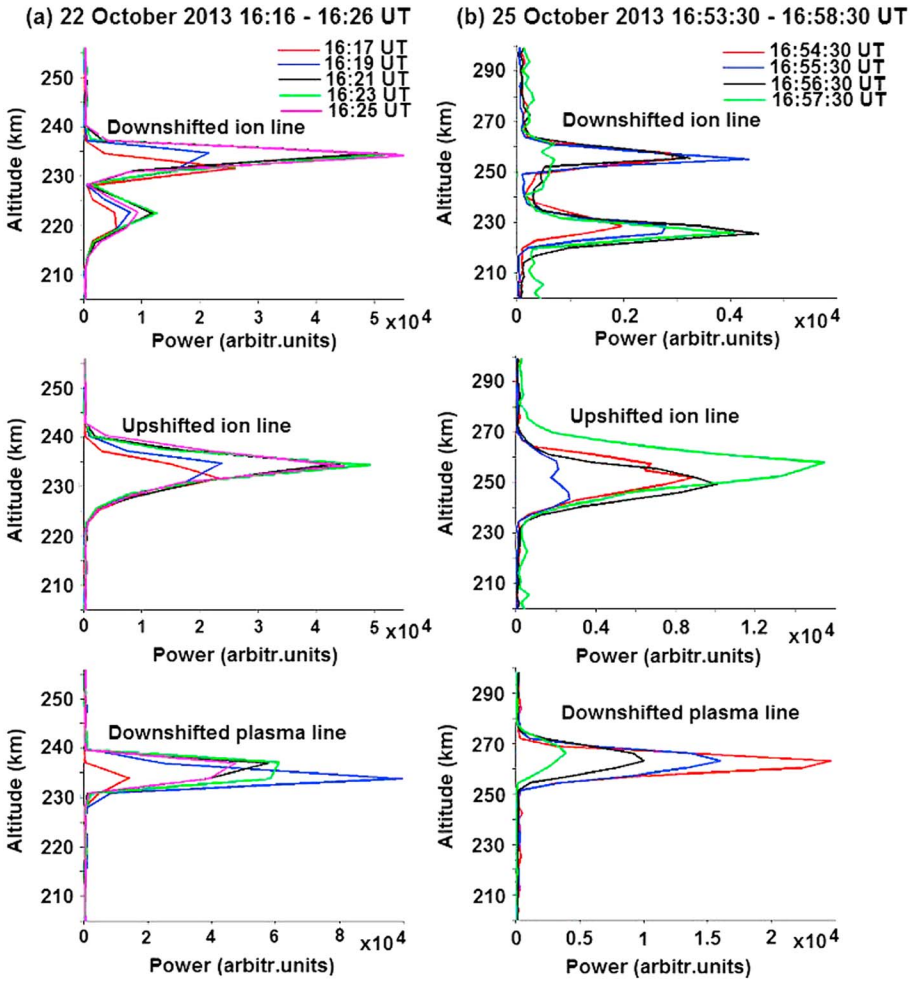

Figure 9. Altitude profiles of the maximum power of HF-enhanced downshifted and upshifted ion lines and downshifted plasma line obtained from EISCAT UHF radar observations for the same HF heater pulses as in Figures 7 and 8. (a) Altitude profiles on 22 October 2013 for HF heater pulse from 16:16 to 16:26 UT ($f_H < f_oF_2$) at 16:17, 16:19, 16:21, 16:23, and 16:25 UT. (b) Altitude profiles on 25 October 2013, for HF heater pulse 16:53:30–16:58:30 UT ($f_H > f_oF_2$) at 16:54:30, 16:55:30, 16:56:30, and 16:57:30 UT.

$I_{577.7}/I_{630.0} = 0.22–0.33$, which is less than with *X*-mode heating, when the ratio $I_{577.7}/I_{630.0} = 0.35–0.5$. Moreover, the *X*-mode RIOEs were excited at lower altitude as compared with the *O*-mode emission. This agrees with the reflection heights for *X*-and *O*-mode heater waves. The lower altitude would assume more collisions, allowing more atomic oxygen atoms in the (^{1}D) state to be quenched due to collisions before they would emit a 630.0 nm photon and therefore increasing the 557.7 nm to 630.0 nm intensity ratio.

O-mode radio-induced optical emissions were accompanied by strong electron temperature enhancements (up to 3 times above the background *Te* level), the generation of the ion outflows from the ionosphere, and the excitation of intense DM component in the SEE spectra. For *X*-mode HF-induced optical emissions, by contrast, the electron temperature increases were much less (only 30% above the background values), the ion outflows and the DM component in the SEE spectra were not generated. The typical feature, observed in all *X*-mode experiments, was the strong apparent electron density enhancements in the field-aligned direction in a wide altitude range up to the upper limit of UHF radar measurements (600 km). The proper estimations of *Ne* cannot be made in the altitude range in which the strong ion acoustic waves are excited due to the high residual to the fitting. However, the large *Ne* enhancements were also observed above these altitudes. The origin of such large *Ne* increases is not clear. We cannot exclude that the intense Langmuir turbulence excited by an *X*-mode HF pump wave could produce fluxes of accelerated electrons that, in turn,

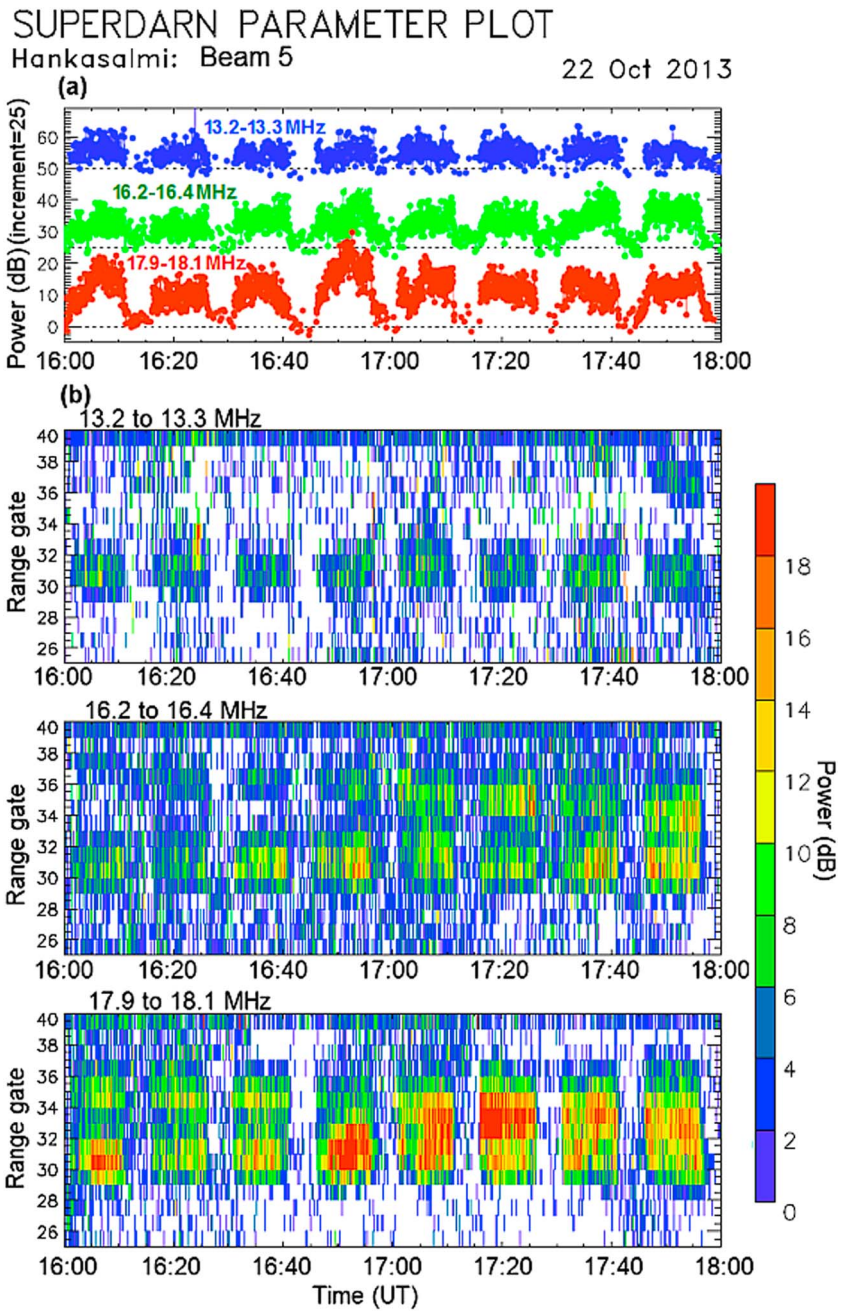

Figure 10. CUTLASS Finland (SuperDARN) radar observations (beam 5) for the HF pumping experiment on 22 October 2013. (a) Averaged backscatter from the HF-produced ionospheric patch at different frequencies (about 10, 13, and 16 MHz). (b) Backscatter from artificial field-aligned irregularities at the same frequencies depending on range gate and time. HF heater details are the same as in Figure 2.

lead to the enhanced production of ionization [*Carlson et al.*, 1982]. The UHF radar observations (see section 2.3) clearly demonstrated that the altitude of the maximum HF-enhanced ion and plasma line intensity from UHF radar measurements closely corresponded to the height of the maximum artificial optical emissions intensity. The other unusual feature for the *X*-mode heater pulse on 19 October 2012 was the appearance of a nonshifted spectral component (at zero frequency) in the ion line spectra (see Figure 4b). This spectral component in the incoherent radar spectra could be a signature of the oscillating two-stream instability (OTSI). Under *O*-mode heating the OTSI is excited due to a four-wave interaction coupling the electromagnetic pump wave to two oppositely propagating Langmuir waves and a nonpropagating ion mode [*Kuo et al.*, 1997].

Similar to a PDI, an OTSI acts over timescales of only a few milliseconds after HF pump on. Further, the PDI and OTSI are normally quenched within seconds due to the TPI excitation, leading to the fully established artificial field-aligned irregularities (FAIs) [e.g., *Stubbe*, 1996]. Under *X*-mode heating the PDI and OTSI were excited throughout the whole heater pulse and coexisted with intense small-scale artificial field-aligned irregularities and *Ne* enhancements.

Experimental results obtained on 22 and 25 October 2013 for the heater frequency f_H = 7.1 MHz have demonstrated that radio-induced optical emissions were excited, when $f_H < f_oF_2$ and $f_H > f_oF_2$. We have compared the behaviors of HF-induced ion and plasma lines at the same heater frequency (f_H = 7.1 MHz) when it is below and above the critical frequency f_oF_2 (see Figures 7–9). As a whole, the HF-induced plasma and ion lines exhibit similar behavior in both cases. However, they were observed in a wider altitude range for the case when $f_H > f_oF_2$ (220–270 km) as compared with the $f_H < f_oF_2$ case (215–240 km). The distinctive feature in the altitude distribution of the downshifted ion lines is the appearance of two power maxima at different altitudes (bottomside and topside echoes), which can be recognized in both cases when $f_H < f_oF_2$ and $f_H > f_oF_2$ (see Figures 9a and 9b). The nonshifted spectral component at zero frequency in the ion line spectra, which can be clearly identified at f_H = 6.2 MHz on 19 October 2012, was not observed at f_H = 7.1 MHz on 22 and 25 October 2013.

On 22 October 2013 optical observations were carried out by the DASI-2 camera at Tromsø and ALIS camera at Abisco station. The DASI-2 does not allow the determination of the altitude distribution of radio-induced optical emissions, but it is possible to do that from the ALIS camera at Abisco. For example, in the heater pulse from 16:16 to 16:26 UT, the most intense radio-induced optical emissions were imaged in the altitude range of 215–240 km (Figure 2b). EISCAT UHF radar observations (Figures 2b and 9a) have shown that in the same altitude range the most intense HF-induced ion and plasma lines were excited.

An *X*-mode HF pump wave is reflected below the upper hybrid resonance height; therefore, it should not excite the TPI and produce well-known phenomena, normally observed under *O*-mode HF pumping, such as strong thermal electron heating, FAIs, and radio-induced optical emissions. However, it was theoretically demonstrated that HF pump wave with *X* polarization can excite upper hybrid plasma oscillations and enhancements of low-frequency plasma perturbations through HF pump-induced scattering by ions [*Vas'kov and Ryabova*, 1998].

The EISCAT UHF radar spectra clearly show HF-enhanced downshifted and upshifted ion lines (ion acoustic waves, IAW) and downshifted plasma lines (Langmuir waves, LW) induced by an *X*-polarized pump wave. It is direct evidence for the excitation of the parametric decay instability (PDI) when the HF pump wave decays into electrostatic plasma waves such as Langmuir and ion acoustic waves. Moreover, the appearance of unshifted component in the ion line spectra (Figure 4b) points to the excitation of OTSI. In principle, an extraordinary (*X* mode) HF pump wave should not excite the longitudinal electrostatic plasma waves, because its electric field and wave vector is oriented transverse to the magnetic field. The excitation of Langmuir waves, responsible for the electron acceleration and enhanced production of ionization [*Carlson et al*., 1982], necessitates the orientation of the wave vector and electric field of HF pump wave parallel to the magnetic field. This is realized at the reflection altitude of *O*-polarized HF pump wave. In such a case we could suggest that there is an effective unknown interaction coupling the *X*-polarized electromagnetic HF pump wave to produce the PDI/OTSI. If, in accordance with *Vas'kov and Ryabova* [1998], the HF pump wave with *X* polarization can excite upper hybrid plasma oscillations, then, as it was shown by *Kuo et al*. [1997], Langmuir waves can be directly excited by upper hybrid (UH) waves. These Langmuir waves could give rise to the acceleration of electron flux, the production of enhanced ionization, and excitation of HF-induced optical emissions.

It is important that the *X*-mode HF-induced ion and plasma lines were observed in a wide altitude extent and were much stronger than the *O*-mode effects. The altitude of their maximum corresponded to the height where the intensity of the RIOE was maximized. Thus, we can suggest the mechanism of many times repeated electron acceleration. Further clarification and theoretical background are needed to explain the origin of unusually strong phenomena excited in the ionospheric *F* region by *X*-polarized HF pump waves.

4. Summary

It was shown for the first time that at high heater frequencies (6.2 and 7.1 MHz) under quiet magnetic conditions, an *X*-polarized HF pump wave can generate the radio-induced optical emissions at red (630 nm)

and green (557.7 nm) lines. Intensities at red and green lines varied through the range of 110–950 R and 50–350 R, respectively, with the ratio of green ($I_{577.7}$) to red ($I_{630.0}$) line of $I_{577.7}/I_{630.0} = 0.35–0.5$. A distinctive feature of *X*-mode artificial optical emissions is their coexistence with intense HF-induced ion and plasma lines and strong small-scale artificial field-aligned irregularities. The altitude of their maximum power corresponded to the height where the intensity of the radio-induced optical emission also maximized. The experimental results obtained have shown that the radio-induced optical emissions can be excited when $f_H < f_oF_2$ and $f_H > f_oF_2$. A comparison between behaviors of HF-induced ion and plasma lines at the same heater frequency (f_H = 7.1 MHz) when it is below and above the critical frequency f_oF_2 was made. Generally, the HF-induced plasma and ion lines exhibit similar behavior in both cases. It is noteworthy that the parametric decay instability was not quenched by fully established FAIs as would normally be the case for *O*-mode pumping. We suggest that the mechanism of repeated electron acceleration by Langmuir turbulence is realized.

Comparison between the *O*- and *X*-mode optical and ionospheric phenomena for a heater frequency lying near the critical frequency ($f_H \approx f_oF_2$) has clearly demonstrated the distinction between the *O*- and *X*-mode effects. The intensity of *X*-mode artificial optical emissions was less compared with *O*-mode emissions, but the higher ratio of green to red lines is typical for them. HF-induced ion and plasma lines were observed in a wide altitude extent and were much stronger (by 3 orders of magnitude) than the *O*-mode effects. The *O*-mode radio-induced optical emission was accompanied by the strong thermal electron heating and generation of ion outflows from the ionosphere. The *Te* values increased from about 1000 K just before the heater-on to 3000 K (at the altitude of 390 km) during the *O*-mode heater pulse. The ion velocities reached 230 m s^{-1} at the height of 523 km. The intense DM component in the SEE spectra was also excited. For *X*-mode radio-induced optical emissions, by contrast, the *Te* increases were much less (only 30% above the background values), the ion outflows and the DM component in the SEE spectra were not generated. There were no significant changes in the ion temperatures for both *O*- and *X*-mode heating. The typical feature, observed in all *X*-mode experiments, was the apparent strong electron density enhancements, by 50–70% above the background *Ne* level, in the magnetic field-aligned direction in a wide altitude range. We note that at altitudes occupied by ion acoustic waves proper *Ne* estimations cannot be made due to the high residual to the fitting. However, the large *Ne* enhancements were also observed above these altitudes. It could be suggested that the Langmuir turbulence excited by an *X*-mode HF pump wave could produce fluxes of accelerated of electrons that, in turn, lead to the enhanced production of ionization.

Further experimental and theoretical investigations of unexpected and unusually strong phenomena in the high latitudinal *F* region of the ionosphere due to *X*-mode HF pump wave are called for.

Acknowledgments

EISCAT is an international scientific association supported by research organizations in China (CRIRP), Finland (SA), Japan (NIPR and STEL), Norway (NFR), Sweden (VR), and the United Kingdom (NERC). CUTLASS is supported by the UK Science and Technology Facilities Council grant PP/E007929/1, the Finnish Meteorological Institute, and the Swedish Institute of Space Physics. T.K.Y. is supported by Science and Technology Facilities Council grant ST/H002480/1. We acknowledge A. Senior who operated the DASI-2 camera and provided calibrated optical data. We also thank M. Rietveld for the help with EISCAT HF pumping experiments and useful discussion. The data used in this paper are available through the EISCAT Madrigal database (http://www.eiscat.se/madrigal/).

Alan Roger thanks Bengt Eliasson and another reviewer for their assistance in evaluating this paper.

References

Ashrafi, M., M. J. Kosch, K. Kaila, and B. Isham (2007), Spatiotemporal evolution of radio wave pump-induced ionospheric phenomena near the fourth electron gyroharmonic, *J. Geophys. Res.*, *112*, A05314, doi:10.1029/2006JA011938.

Bernhardt, P. A., C. A. Tepley, and L. M. Duncan (1989), Airglow enhancements associated with plasma cavities formed during ionospheric heating experiments, *J. Geophys. Res.*, *94*, 9071–9092, doi:10.1029/JA094iA07p09071.

Blagoveshchenskaya, N. F., T. D. Borisova, T. Yeoman, M. T. Rietveld, I. M. Ivanova, and L. J. Baddeley (2011), Artificial field-aligned irregularities in the high-latitude F region of the ionosphere induced by an X-mode HF heater wave, *Geophys. Res. Lett.*, *38*, L08802, doi:10.1029/2011GL046724.

Blagoveshchenskaya, N. F., T. D. Borisova, T. K. Yeoman, M. T. Rietveld, I. Häggström, and I. M. Ivanova (2013), Plasma modifications induced by an X-mode HF heater wave in the high latitude F region of the ionosphere, *J. Atmos. Sol. Terr. Phys.*, *105-106*, 231–244.

Brändström, B. U. E., T. B. Leyser, Å. Steen, M. T. Rietveld, B. Gustavsson, T. Aso, and M. Ejiri (1999), Unambiguous evidence of HF pump-enhanced airglow, *Geophys. Res. Lett.*, *26*, 3561–3564, doi:10.1029/1999GL010693.

Brändström, U. (2003), The Auroral large imaging system—Design, operation and scientific results, *IRF Scientific Rep.*, *279*, PhD thesis, Swedish Institute of Space Physics, Kiruna, Sweden.

Bryers, C., M. Kosch, A. Senior, M. T. Rietveld, and T. K. Yeoman (2013), The thresholds of ionospheric plasma instabilities pumped by high-frequency radio waves at EISCAT, *J. Geophys. Res. Space Physics*, *118*, 7472–7481, doi:10.1002/2013JA019429.

Carlson, H. C., V. B. Wickwar, and G. P. Mantas (1982), Observations of fluxes of suprathermal electrons accelerated by HF excited instabilities, *J. Atmos. Sol. Terr. Phys.*, *44*, 1089–1100.

DuBois, D. F., H. A. Rose, and D. Russell (1990), Excitation of strong Langmuir turbulence in plasmas near critical density: Application to HF heating of the ionosphere, *J. Geophys. Res.*, *95*, 21,221–21,272, doi:10.1029/JA095iA12p21221.

Fejer, J. A. (1979), Ionospheric modification and parametric instabilities, *Rev. Geophys. Space Phys.*, *17*(1), 135–153.

Frolov, V. L., L. M. Kagan, E. N. Sergeev, G. P. Komrakov, P. A. Bernhardt, J. A. Goldstein, L. S. Wagner, C. A. Selcher, and P. Stubbe (1999), Ionospheric observations of F region artificial plasma turbulence, modified by powerful X-mode radio waves, *J. Geophys. Res.*, *104*, 12,695–12,704, doi:10.1029/1998JA900182.

Grach, S. M., and V. Y. Trakhtengerts (1975), Parametric excitation of ionospheric irregularities extended along the magnetic field, *Radiophys. Quant. Electron.*, *18*, 951–957.
Gurevich, A., K. Zybin, H. Carlson, and T. Pedersen (2002), Magnetic zenith effect in ionospheric modifications, *Phys. Lett. A*, *305*(5), 264–274.
Gurevich, A. V. (2007), Nonlinear effects in the ionosphere, *Phys.-Uspekhi*, *50*, 1091–1121.
Gurevich, A. V., H. C. Carlson, Y. V. Medvedev, and K. R. Zybin (2004), Langmuir turbulence in ionospheric plasma, *Plasma Phys. Rep.*, *30*, 995–1005.
Gustavsson, B., and B. Eliasson (2008), HF radio wave acceleration of ionospheric electrons: Analysis of HF-induced optical enhancements, *J. Geophys. Res.*, *113*, A08319, doi:10.1029/2007JA012913.
Gustavsson, B., T. Sergienko, M. T. Rietveld, F. Honary, Å. Steen, B. U. E. Brändström, T. B. Leyser, A. L. Aruliah, T. Aso, and M. Ejiri (2001), First tomographic estimate of volume distribution of enhanced airglow emission caused by HF pumping, *J. Geophys. Res.*, *106*, 29,105–29,123, doi:10.1029/2000JA900167.
Gustavsson, B., B. U. E. Brändström, Å. Steen, T. Sergienko, T. B. Leyser, M. T. Rietveld, T. Aso, and M. Ejiri (2002), Nearly simultaneous images of HF-pump enhanced airglow at 6300 Å and 5577 Å, *Geophys. Res. Lett.*, *29*(24), 2220, doi:10.1029/2002GL015350.
Gustavsson, B., T. B. Leyser, M. Kosch, M. T. Rietveld, Å. Steen, B. U. E. Brändström, and T. Aso (2006), Electron gyroharmonic effects in ionization and electron acceleration during high-frequency pumping in the ionosphere, *Phys. Rev. Lett.*, *97*, 195002, doi:10.1103/PhysRevLett.97.195002.
Gustavsson, B., R. Newsome, T. B. Leyser, M. J. Kosch, L. Norin, M. McCarrick, T. Pedersen, and B. J. Watkins (2009), First observations of X-mode suppression of O-mode HF enhancements at 6300 Å, *Geophys. Res. Lett.*, *36*, L20102, doi:10.1029/2009GL039421.
Kosch, M. J., M. T. Rietveld, A. J. Kavanagh, C. Davis, T. K. Yeoman, F. Honary, and T. Hagfors (2002), High-latitude pump-induced optical emissions for frequencies close to the third electron gyro-harmonic, *Geophys. Res. Lett.*, *29*(23), 2112, doi:10.1029/2002GL015744.
Kosch, M. J., T. Pedersen, M. T. Rietveld, B. Gustavsson, S. M. Grach, and T. Hagfors (2007a), Artificial optical emissions in the high latitude thermosphere induced by powerful radio waves: An observational review, *Adv. Space Res.*, *40*, 365–376.
Kosch, M. J., T. Pedersen, E. Mishin, S.-I. Oyama, J. Hughes, A. Senior, B. Watkins, and B. Bristow (2007b), Coordinated optical and radar observations of ionospheric pumping for a frequency pass through the second electron gyro-harmonic at HAARP, *J. Geophys. Res.*, *112*, A06325, doi:10.1029/2006JA012146.
Kuo, S., M. Lee, and P. Kossey (1997), Excitation of oscillating two stream instability by upper hybrid pump in ionospheric heating experiments at Tromsø, *Geophys. Res. Lett.*, *24*, 2969–2972, doi:10.1029/97GL03054.
Lehtinen, M. S., and A. Huuskonen (1996), General incoherent scatter analysis and GUISDAP, *J. Atmos. Sol. Terr. Phys.*, *58*, 435–452.
Lester, M., et al. (2004), Stereo CUTLASS: A new capability for the SuperDARN radars, *Ann. Geophys.*, *22*, 459–473.
Leyser, T. B. (2001), Stimulated electromagnetic emissions by high-frequency electromagnetic pumping of the ionospheric plasma, *Space Sci. Rev.*, *98*, 223–328.
Leyser, T. B., B. Gustavsson, B. U. E. Brändström, F. Honary, A. Steen, T. Aso, M. T. Rietveld, and M. Ejiri (2000), Simultaneous measurements of high-frequency pump-enhanced airglow and ionospheric temperatures at auroral latitudes, *Adv. Polar Up. Atmos. Res.*, *14*, 1–11.
Mishin, E. V., W. J. Burke, and T. Pedersen (2005a), HF-induced airglow at magnetic zenith: Theoretical considerations, *Ann. Geophys.*, *23*, 47–53.
Mishin, E. V., M. J. Kosch, T. R. Pedersen, and W. J. Burke (2005b), HF-induced airglow at magnetic zenith: Thermal and parametric instabilities near electron gyroharmonics, *Geophys. Res. Lett.*, *32*, L23106, doi:10.1029/2005GL023864.
Pedersen, T., and H. Carlson (2001), First observations of HF heater-produced airglow at the High Frequency Active Auroral Research Program facility: Thermal excitation and spatial structuring, *Radio Sci.*, *36*, 1013–1026, doi:10.1029/2000RS002399.
Pedersen, T. R., M. McCarrick, E. Gerken, C. Selcher, D. Sentman, H. C. Carlson, and A. Gurevich (2003), Magnetic zenith enhancement of HF radio-induced airglow production at HAARP, *Geophys. Res. Lett.*, *30* (A4), 1169, doi:10.1029/2002GL016096.
Pedersen, T. R., B. Gustavsson, E. Mishin, E. MacKenzie, H. C. Carlson, M. Starks, and T. Mills (2009), Optical ring formation and ionization production in high-power HF heating experiments at HAARP, *Geophys. Res. Lett.*, *36*, L18107, doi:10.1029/20009GL040047.
Perkins, F. W., C. Oberman, and E. J. Valco (1974), Parametric instabilities and ionospheric modification, *J. Geophys. Res.*, *79*, 1478–1496, doi:10.1029/JA079i010p01478.
Rietveld, M. T., H. Kohl, H. Kopka, and P. Stubbe (1993), Introduction to ionospheric heating at Tromsø—I. Experimental overview, *J. Atmos. Sol. Terr. Phys.*, *55*, 577–599.
Rietveld, M. T., M. J. Kosch, N. F. Blagoveshchenskaya, V. A. Kornienko, T. B. Leyser, and T. K. Yeoman (2003), Ionospheric electron heating, aurora and striations induced by powerful HF radio waves at high latitudes: Aspect angle dependence, *J. Geophys. Res. 108*(A4), 1141, doi:10.1029/2002JA009543.
Rishbeth, H., and T. van Eyken (1993), EISCAT: Early history and the first ten years of operation, *J. Atmos. Sol. Terr. Phys.*, *55*, 525–542.
Robinson, T. R. (1989), The heating of the high latitude ionosphere by high power radio waves, *Phys. Rep.*, *179*, 79–209.
Robinson, T. R., A. J. Stocker, G. E. Bond, P. Eglitis, D. M. Wright, and T. B. Jones (1997), O- and X-mode heating effects observed simultaneously with the CUTLASS and EISCAT radars and low power HF diagnostics at Tromsø, *Ann. Geophys.*, *15*, 134–136.
Senior, A., M. T. Rietveld, I. Häggström, and M. J. Kosch (2013), Radio-induced incoherent scatter ion line enhancements with wide altitude extents in the high-latitude ionosphere, *Geophys. Res. Lett.*, *40*, 1669–1674, doi:10.1002/grl.50272.
Stubbe, P. (1996), Review of ionospheric modification experiments at Tromso, *J. Atmos. Sol. Terr. Phys.*, *58*, 349–368.
Stubbe, P., H. Kopka, and B. Thidé (1984), Stimulated electromagnetic emission: A new technique to study the parametric decay instability in the ionosphere, *J. Geophys. Res.*, *89*, 7523–7536, doi:10.1029/JA089iA09p07523.
Stubbe, P., H. Kohl, and M. T. Rietveld (1992), Langmuir turbulence and ionospheric modification, *J. Geophys. Res.*, *97*, 6285–6297, doi:10.1029/91JA03047.
Vas'kov, V. V., and A. V. Gurevich (1976), Nonlinear resonant instability of a plasma in the field of an ordinary electromagnetic wave, *Sov. Phys. JETP. Engl. Transl.*, *42*, 91–97.
Vas'kov, V. V., and N. A. Ryabova (1998), Parametric excitation of high frequency plasma oscillations in the ionosphere by a powerful extraordinary radio wave, *Adv. Space Res.*, *21*, 697–700.